Journal of Solid State Chemistry **149,** 68–74 (2000)
Article ID jssc.1999.8497, available online at http://www.idealibrary.com on IDEAL®

Structure Analysis of Tantalum Chloride–Graphite Intercalation Compound Using Molecular Simulations

Pavla Čapková* and Jürgen Walter†

*Faculty of Mathematics and Physics, Charles University Prague, Ke Karlovu 3, CZ-12116 Prague, Czech Republic; and
†Osaka National Research Institute, AIST, MITI, 1-8-31 Midorigaoka, Ikeda, Osaka 563-8577, Japan

Structure analysis of graphite intercalated with $TaCl_6^-$ and $TaOCl_3$ has been carried out using molecular mechanics simulations and compared to previously published experimental data obtained by X-ray powder diffraction, electron diffraction, and other techniques. The basal spacing calculated for the second stage of graphite intercalated with tantalum(V) chloride c_2(calc) = 12.80 Å was in agreement with the experimental value c_2(exp) = 12.79 Å obtained from X-ray powder diffraction. Modeling revealed the two-dimensional ordering of $TaCl_6^-$ octahedra in the interlayer space of graphite lattice. This ordered interlayer structure of $TaCl_6^-$ is incommensurate with the graphite lattice and can be described as the two-dimensional space group 17*pm*6, hexagonal plane lattice with the lattice parameter 6.54 Å. The simulated electron diffraction pattern for calculated structure was in good agreement with that seen in the experiment. The guest layer lattice parameter obtained from electron diffraction was 6.5 Å. The simulations gave evidence that this guest structure can be obtained only with $TaCl_6^-$ octahedra as guests; other possible guests—$TaCl_5$ dimers—can be definitely excluded. In case of tantalum oxychloride the fragments of $TaOCl_3$ chain structure are arranged in the interlayer space, giving the basal spacing of the second stage c_2(calc) = 13.39 Å.

INTRODUCTION

Graphite intercalation compounds (GICs) possess remarkable physical and chemical properties, which make these compounds interesting for numerous practical applications: catalysts, oxidation inhibitors, ionic conductors, conductors with metallic conductivity and low density, etc. (see, for example, (1, 2)). The distinctive property of GICs is that a given intercalant is able to form compounds with a periodic sequence of n host layers of graphite and one intercalant layer of guest species. The number of n defines the "stage" of the compound (2). While the staging order and interlayer distances can be determined by X-ray powder diffraction, the determination of the in-plane structure of guest layers is difficult, due to the disorder in layer stacking. The X-ray powder diffraction pattern is also affected with the strong preferred orientation of disk-shaped particles. In recent years various complementary experimental methods have been used to determine the in-plane structure of GICs: magic-angle spinning nuclear magnetic resonance (MAS-NMR) (3), X-ray photoelectron spectroscopy (XPS) (4), X-ray absorption spectroscopy (EXAFS and XANES) (5), scanning tunneling microscopy (STM) (6), selected-area electron diffraction (SAED) (7), and atomic force microscopy (AFM) (8). Graphite forms intercalation compounds with a wide variety of metal chlorides. These compounds exhibit different arrangements of guest species in the interlayer space of graphite lattice, as a result of the competition of host–guest and guest–guest interactions. Behrens and Metz 1989 (9) proposed a classification scheme based on the topology of the in-plane structure for GICs intercalated with metal chlorides: (i) zero-dimensional intercalates, where the guest layer is built up from molecules or ions (graphite intercalated with $AlCl_3$, $SbCl_5$, $SnCl_4$, $MoCl_5$, $GaCl_3$, etc), (ii) one-dimensional intercalates whose guest layers are constructed from chains (graphite intercalated with $PdCl_2$, etc), (iii) two-dimensional intercalates with guest layers which show strong bonding forces in two directions, i.e., guest layer with strong covalent interlayer bonds (graphite intercalated with $ZnCl_2$, $MnCl_2$, $FeCl_3$, etc.).

In the present study we investigate the GIC with tantalum chloride and tantalum oxy-chloride using molecular mechanics simulations. X-ray powder diffraction study of tantalum chloride–GIC (10) showed the basal spacing for the second stage 12.79 Å. An ordered in-plane structure of guest layer has been observed by the SAED and STM methods (11). Electron microprobe data, EMPA (12), of environmentally aged $TaCl_5$–GICs showed in the center of particles the Cl/Ta ratio of approximately 6 (the additional chlorine came from the chlorine atmosphere by the formation). Near cracks in the basal plane and near prismatic edges the tantalum oxychloride ($TaOCl_3$), as an intermediate product of hydrolysis has been observed by EMPA (12) and by particle-induced X-ray emission, PIXE (13).

In solid state the tantalum(V) chloride ($TaCl_5$) forms dimers with two octahedra sharing one common edge.

0022-4596/00 $35.00

Experimental results obtained till this time (EMPA data (12)) did not give the clear evidence of the nature of intercalated species, which means that no determination could be made between the $TaCl_6^-$ octahedra and $TaCl_5$ dimers with an excess on chlorine bonded to the host lattice. The aim of the present study is to determine the in-plane structure of guest species and to decide which guest species is intercalated inside an as-prepared $TaCl_5$–GIC. To answer this question, the following possible guest species were considered: $TaCl_6^-$ octahedra, dimeric $TaCl_5$, and fragments of $TaOCl_3$ structure.

Present structure analysis is based on combination of molecular mechanics simulations in the Cerius^2 modeling environment, with X-ray powder diffraction and electron diffraction. The crystal energy in molecular mechanics simulations is described by an empirical force field. The potential energy for an arbitrary geometry of a molecule or crystal structure is expressed as a superposition of valence (bonded) interactions and nonbonded interactions (i.e., Van der Waals, Coulombic, and hydrogen bond). The valence interactions consist of bond stretch, bond-angle bend, torsion, and inversion terms (for more details see (14); for a description of Cerius^2 software, see (15)). The strategy of modeling in the present study, i.e., the building of the initial model, the setting up of the energy expression, the parametrization of the model, and minimization strategy, was based on the experiment (XRD, electron diffraction, electron microprobe analysis (EMPA), and STM).

STRATEGY OF MODELING

Strategy of modeling is based on the experimental results of X-ray powder diffraction (10) and SAED combined with STM data (11). The initial models have been built using the known structure of graphite (space group $P6_3/mmc$ $a = b = 2.454$ Å, $c = 6.70$ Å, $\alpha = \beta = 90°$, $\gamma = 120°$).

Initial Model with $TaCl_6^-$ Octahedra

According to the result of X-ray powder diffraction (10), the identity period has been set up to 12.79 Å for the intercalation of tantalum chloride. The measured composition (12) of tantalum chloride–GIC for the fresh stage 2 corresponding to the formula $C_{27}TaCl_{5.3-6.0}$ leads to the assumption that there may be individual octahedra $TaCl_6^-$ in the interlayer space. To keep this composition and to create a supercell of reasonable size for calculations we have built the supercell $8a \times 8b \times 1c$, where $c = 12.79$ Å and the $a = b$ is the parameter of the graphite unit cell. Nine $TaCl_6^-$ octahedra have been inserted into the interlayer space of graphite, corresponding to the composition $C_{28.4}TaCl_6$, which represents a reasonable compromise between the accuracy of the model and supercell size (with respect to the computational time). The Ta–Cl bond distances of 2.30 Å in undistorted $TaCl_6^-$ octahedra have been taken from Ref. (14), where two isomorphous structures, $NbCl_5$ and $TaCl_5$, have been determined. Graphite layers and $TaCl_6^-$ octahedra have been treated as rigid units during energy minimization. Ten rigid units have been assigned to the initial model (in supercell $8a \times 8b \times 1c$): nine $TaCl_6^-$ octahedra and one double layer of graphite between guest layers. The host–guest and guest–guest interactions have been described using nonbond terms only (i.e., van der Waals and electrostatic).

Initial Model with $TaCl_5$ Dimers

Four $TaCl_5$ dimers have been placed in the interlayer space of the supercell $6a \times 9b \times 12.79$ Å, containing the 54 graphite unit cells, corresponding to the composition $C_{27}TaCl_5$. The structure of $TaCl_5$ dimers have been taken from the work (14), which presents two isomorphous structures of $NbCl_5$ and $TaCl_5$. The same strategy of minimization, as in the case of $TaCl_6^-$ octahedra has been used for dimeric tantalum chloride, i.e., the nonbond interactions between rigid units. Five rigid units have been assigned to this supercell: four dimers and a double graphite layer between the host layers.

Initial Model with $TaOCl_3$

The initial model for the graphite intercalated with tantalum oxychloride has been built as a supercell containing 100 graphite unit cells, i.e., $10a \times 10b \times 1c$. Two fragments of the chain structure of $TaOCl_3$ (see Fig. 1) have been placed

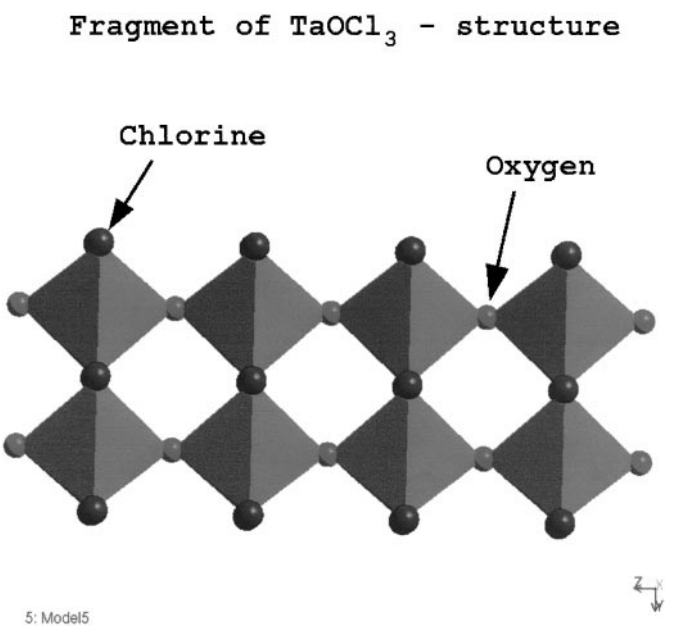

FIG. 1. Fragment of $TaOCl_3$ structure, intercalated into the interlayer space of graphite.

into this supercell corresponding to the composition $C_{25}O_{1.25}Cl_3Ta$. This composition represents the compromise between the size of the supercell built for calculations and the experimentally estimated composition $C_{27}OCl_3Ta$ (12). The $TaOCl_3$ fragments have been built using the structure data (15). The same strategy of minimization as in case of tantalum chloride has been used in this case; that means that the host–guest interactions have been described using nonbond terms only and the guest species—the $TaOCl_3$ fragments and double graphite layers have been treated as rigid units. In both cases the Crystal Packer module in the Cerius^2 modeling environment has been used for energy minimization.

Energy Calculation in Crystal Packer

Crystal Packer is a computational module that estimates the total sublimation energy and packing of molecular crystals. Energy calculations in Crystal Packer take into account the nonbond terms only, i.e., van der Waals interactions (VDW), Coulombic interactions (COUL), hydrogen bonding (H–B), internal rotations, and hydrostatic pressure. The asymmetric unit of the crystal structure is divided into fragment-based rigid units. Nonbond (VDW, COUL, H–B) energies are calculated between the rigid units. During the energy minimization, the rigid units can be translated and rotated and the unit cell parameters varied.

In the present calculations the rigid units were $TaCl_6$ octahedra, $TaCl_5$ dimers, $TaOCl_3$ fragments, and the double graphite layer. The nonbond interaction energy as a sum of VDW, COUL and H–B interaction energy between rigid units has been minimized. This energy related to one supercell is called the total sublimation energy.

The Ewald summation method is used to calculate the Coulombic energy in a crystal structure (16). The Ewald sum constant was 0.5 $Å^{-1}$. The minimum charge taken into the Ewald sum was 0.00001e. All atom pairs with separations less than 10 Å were included in the real-space part of the Ewald sum and all reciprocal-lattice vectors with lengths less than 0.5 $Å^{-1}$ were included in the reciprocal part of the Ewald summation. Charges in the crystal are calculated in Cerius^2 using the QEq-method (charge equilibrium approach). This method is described in detail in the original work, ref. (17). For VDW we used the Lennard–Jones functional form, with the arithmetical radius combination rule. A nonbond cutoff distance for the VDW interactions was 7.0 Å. There are three sets of VDW parameters, available in Crystal Packer: from the Tripos force field (18), from the Universal force field (19), and from the Dreiding force field (20). As the Tripos force field has been developed for organic molecules, we used in the present case the Universal and Dreiding–VDW parameters. As the Dreiding force field has no parameters for tantalum, we had to insert the VDW parameters for Ta-atom taken from Universal force field.

RESULTS AND DISCUSSION

Model with $TaCl_6^-$ Octahedra and $TaCl_5$ Dimers in the Interlayer Space

The structure of graphite intercalated with tantalum chloride, obtained as a result of energy minimization is presented in Fig. 2. Both sets of VDW parameters (Universal and Dreiding) led to the same arrangement of guest molecules, illustrated in Fig. 2; however, the basal spacings of the stage *2* were slightly different: c_2(calc) = 12.80 Å for the Dreiding–VDW parameters and c_2(calc) = 12.74 Å for the Universal–VDW parameters. The total sublimation energy per one supercell, $E_S = 577.33$ kcal/mol, consists of the prevailing VDW contribution, $E_{VWD} = 335.22$ kcal/mol, and the Coulombic contribution, $E_{COUL} = 242.11$ kcal/mol. The corresponding energy values calculated per one graphite unit cell are $E_S = 9.021$ kcal/mol, $E_{VWD} = 5.238$ kcal/mol, and $E_{COUL} = 3.783$ kcal/mol.

The in-plane ordering of $TaCl_6^-$ octahedra is illustrated in Fig. 3 and can be described by the plane group 17*p6m*, hexagonal plane lattice with the lattice parameter 6.54 Å, which is the equilibrium Ta–Ta distance. This type of in-plane guest structure is in agreement with the result of electron diffraction (7). Figures 4a and 4b show the simulated electron diffraction pattern for the calculated model with of $TaCl_6^-$ octahedra for the zone 001(a) and the measured electron diffractogram is in Fig. 4b. As one can

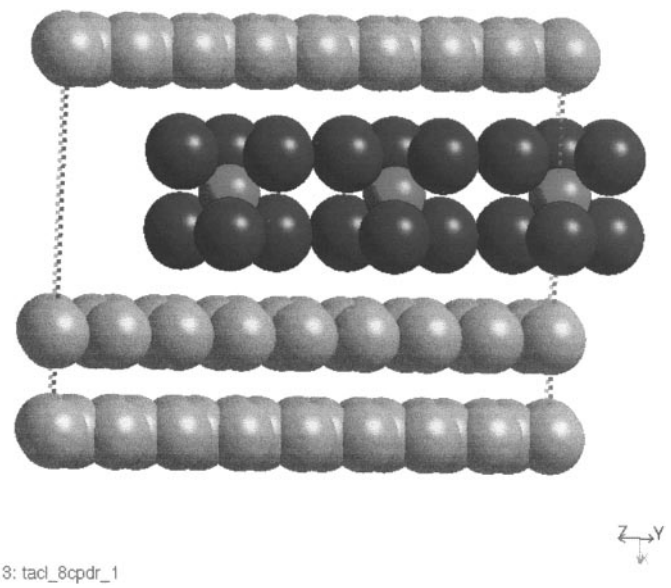

FIG. 2. Arrangement of $[TaCl_6]^-$ octahedra in the interlayer space of graphite; view of one supercell, $8a \times 8b \times 12.80$ Å.

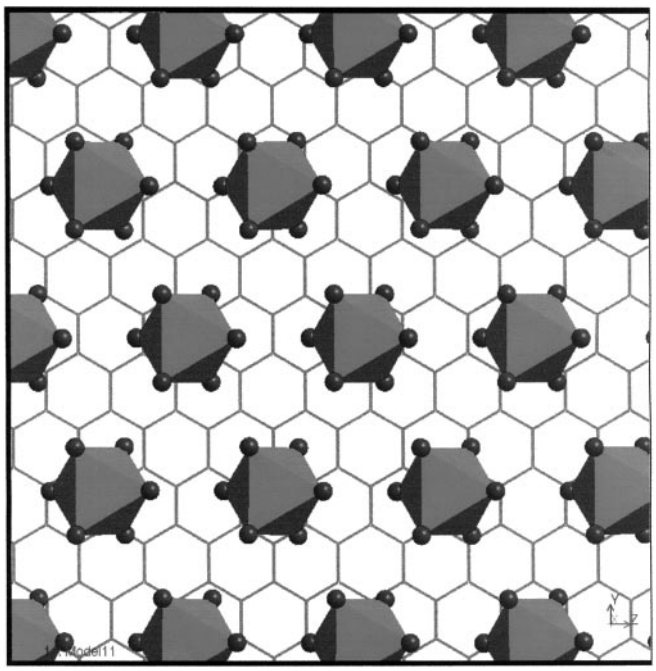

FIG. 3. In-plane ordering of $[TaCl_6]^-$ octahedra in the interlayer space of graphite.

see, both figures show the hexagonal symmetry of the graphite structure and hexagonal symmetry of the guest layer; see the first sixfold ring in the central part of difractogram. The graphite reflections are denoted with asterisks. The angle of the mutual rotation of the host and guest lattice is different in both diffractograms, as there is no possibility in the Cerius Crystal Packer module to create the model of two incommensurate lattices with mutual rotation of both lattices. In spite of this difficulty, the main feature of the guest structure, which means the hexagonal symmetry of the plane lattice, is evident from the comparison of Figs. 4a and 4b. The plane lattice constant estimated from electron diffraction 6.5 Å agrees with the calculated value of 6.54 Å.

The guest layer forms the incommensurate structure with the carbon lattice. The orientation of $TaCl_6^-$ octahedra in the interlayer is evident from Figs. 2 and 3. One face of the octahedron is parallel with the host layers (see Figs. 3 and 4), which means that three chlorine atoms are adjacent to the graphite layer. As one can see from Fig. 3 the mutual positions of the octahedral faces adjacent to graphite layer are not regular, thanks to the incommensurance of host–guest layers; i.e., the chlorine atoms may reside in the middle of the hexagonal graphite rings as well as in various different positions. This effect is observable by the STM patterns (see Fig. 5), where the bright spots corresponding to the chlorine atoms in the middle of the carbon rings shows the irregular distribution (the guest layer is covered with graphite layer in the STM pattern).

The minimization of the initial model with dimeric structure of $TaCl_5$ in the interlayer space led to the higher value of basal spacing, 12.85 Å, using the Tripos force field. (the experimental value is 12.79 Å.) The main disagreement in this case has been observed between the experimental and

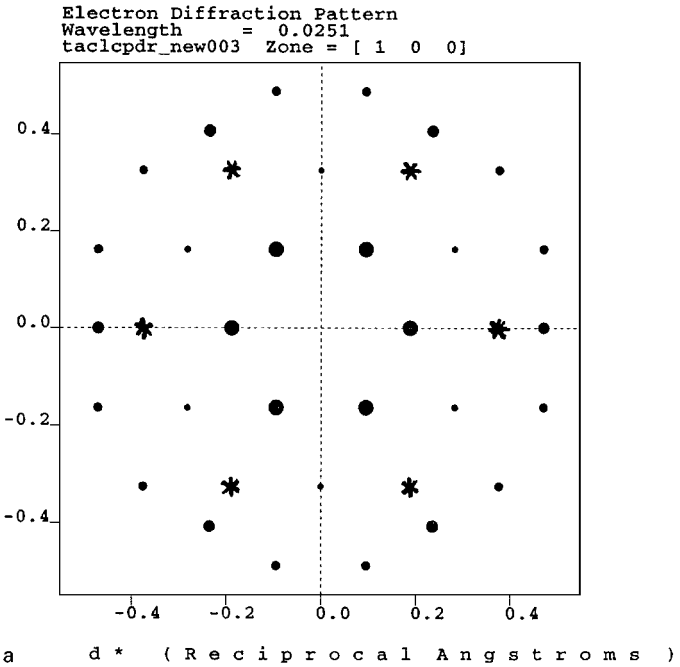

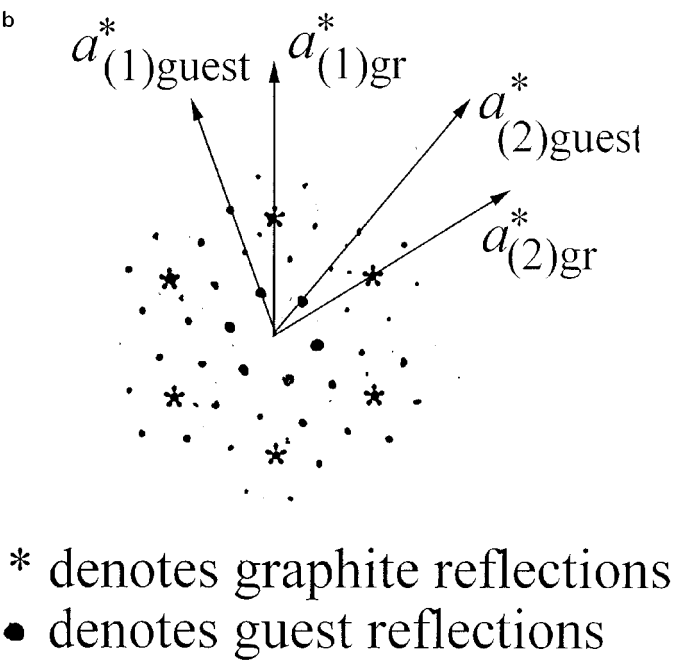

FIG. 4. (a) Simulated and (b) measured electron diffraction pattern for $TaCl_6$–GIC.

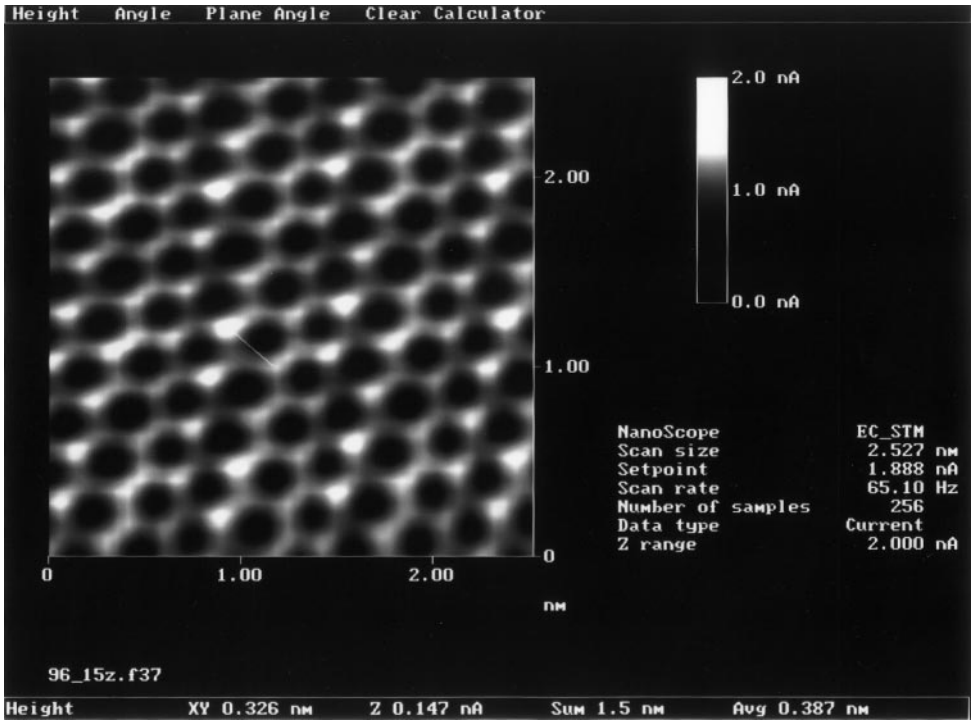

FIG. 5. STM (scanning tunneling microscope) pattern for $TaCl_6$–GIC.

calculated electron diffraction pattern. Calculated electron diffractograms did not show the hexagonal symmetry of the in-plane guest structure and consequently the $TaCl_5$ dimers have been excluded as a guest species.

Model with $TaOCl_3$ in the Interlayer Space

The structure of the graphite intercalated with tantalum oxychloride is shown in Fig. 6a in side view of the supercell and in Fig. 6b in top view, perpendicular to the layers. The basal spacing for this model is $c_2(\text{calc}) = 13.39$ Å. The higher value of the basal spacing obtained for $TaOCl_3$–GIC in comparison with $TaCl_6$–GIC is a result of different orientation of tantalum octahedra in both compounds. While in $TaCl_6$–GIC one face of the Ta octahedron is parallel to the host layers, in $TaOCl_3$–GIC one edge of the Ta octahedron is parallel with the host layer, as one can see comparing the Figs. 3 and 6b. The total sublimation energy per one graphite unit cell is $E_S = 9.021$ kcal/mol, van der Waals contribution $E_{VWD} = 5.238$ kcal/mol, and electrostatic contribution $E_{COUL} = 3.783$ kcal/mol for $TaOCl_3$–GIC. The higher basal spacing for tantalum oxychloride explains the measured increasing of basal spacing in samples exposed to water or to the air humidity.

CONCLUSION

The simulations taking various possible guest species in the consideration demonstrate that for an as-prepared $TaCl_5$–GIC, dimeric $TaCl_5$ can be totally exluded. The as-prepared compound consists of $TaCl_6^-$ octahedra. Only this guest species gives a simulated identity period in the *c*-direction and a simulated in-plane SAED pattern, which fits with experimental XRD (10), STM, and SAED (11) data. Also the chemical composition of $TaCl_6^-$ octahedra is in good agreement with EMPA data (12). In this study an environmentally aged sample was measured; therefore regions with different compositions (partial hydrolyzation) could be observed (12). Regions in the center should be hardly affected by water and they show Cl/Ta ratios ≈ 6.3 (12), which fits with the assumption of $TaCl_6^-$ octahedra as guest. The excess in chlorine in regard to the starting material ($TaCl_5$) is due to the Cl_2 gas atmosphere in the formation of the compound.

Of course the as-prepared compound should not consist of $TaOCl_3$, but the environmentally aged sample may show this guest. The simulated identity period and in-plane SAED pattern makes it easier for further experimental studies to identify such domains.

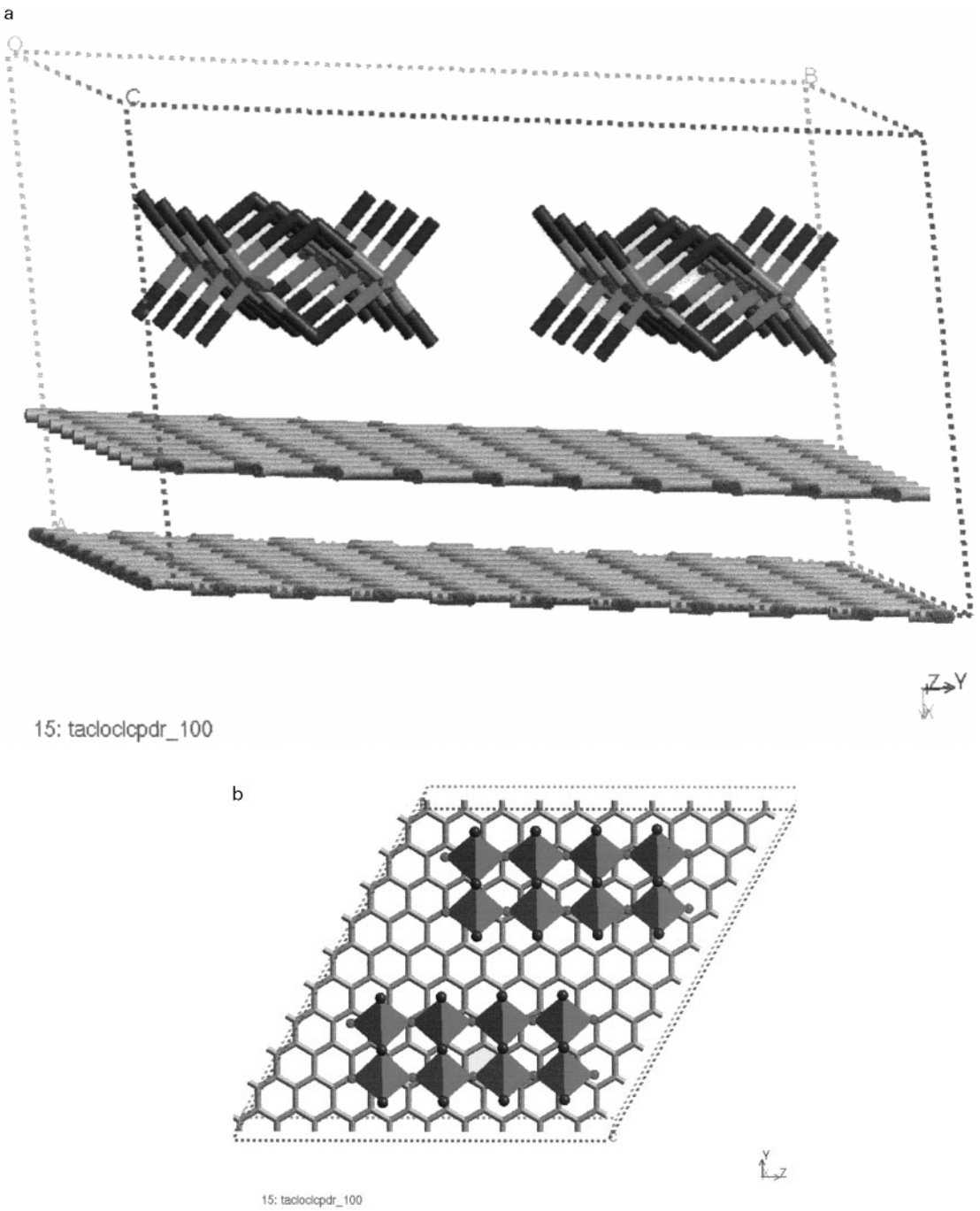

FIG. 6. Graphite intercalated with tantalum oxychloride. (a) Side view of one supercell, $10a \times 10b \times 13.39$ Å, with two $TaOCl_3$ fragments; (b) top view of the arrangement of $TaOCl_3$ fragments in the interlayer space of graphite.

ACKNOWLEDGMENTS

This work was supported by the Grant Agency of the Charles University Prague, Grant GAUK 37/97/B, and Grant Agency of Czech Republic, Grant 203/99/0067. J.W. is grateful to the Alexander von Humboldt foundation (AvH, Germany) and the Science and Technology Agency (STA, Japan) for his Japan fellowship.

REFERENCES

1. S. A. Solin, *in* "Advances in Chemical Physics" (I. Prigogine and Stuart A. Rice, Eds.), pp. 455–530. Wiley, New York, 1982.
2. G. R. Hennig, *in* "Progress in Inorganic Chemistry" (F. A. Cotton, Ed.), Vol. 1, pp. 125–205. Interscience, New York, 1959.

3. K. Sato, M. Noguchi, A. Demachi, N. Oki, and M. Endo, *Science* **264,** 556 (1994).
4. V. Mordkovich, *Synth. Met*. **80,** 243 (1996).
5. P. Behrens, J. Ehrich, W. Metz, and W. Niemann, *Synth. Met*. **34,** 199 (1989).
6. H. P. Lang, R. Wiesendanger, V. Thommen-Geiser, and H. J. Guntherod, *Phys. Rev. B* **45,** 1829 (1992).
7. J. Walter and H. Shioyama, *J. Phys.* **11,** L21 (1999).
8. N. Ikemiya, Y. Okazaki, S. Hara, and T. Nakajima, *Carbon* **32,** 1191 (1994).
9. P. Behrens and W. Metz, *Synth. Met*. **34,** 223 (1989).
10. J. Walter and H. P. Boehm, *Carbon* **33,** 1121 (1995).
11. J. Walter, H. Shioyama, Y. Sawada, and S. Hara, *Carbon* **36,** 1277 (1998).
12. J. Walter, *Synth. Met*. **89,** 39 (1997).
13. J. Walter and M. Maetz, *Mikrochim. Acta* **127,** 183 (1997).
14. A. Zalkin and D. E. Sands, *Acta Crystallogr*. **11,** 615 (1958).
15. D. E. Sands, A. Zalkin, and R. E. Elson, *Acta Crystallogr*. **12,** 21 (1959).
16. N. Karasawa and W. A. J. Goddard III, *J. Phys. Chem.* **93,** 7320 (1989).
17. A. K. Rappé and W. A. Goddard III, *J. Phys. Chem.* **95,** 3358 (1991).
18. M. Clark, R. D. Cramer III, and N. Van Opdenbosh, *J. Comp. Chem.* **10,** 982 (1989).
19. A. K. Rappe, C. J. Casewit, K. S. Colwell, W. A. Goddard, and W. M. Skiff, *J. Am. Chem. Soc*. **114,** 10024 (1992).
20. L. S. Mayo, B. D. Olafson, and W. A. Goddard III, *J. Phys. Chem.* **94,** 8897 (1990).
21. P. Comba and T. W. Hambley, *in* "Molecular Modeling." VCH Verlagsgeseleschaft mbH., Weinheim, New York, 1995.